Journal of Southeast University (English Edition) Vol. 40, No. 3, pp. 295 - 303 Sept. 2024 ISSN 1003—7985

Experimental study on the properties of CMTs-incorporated geopolymers prepared at low temperatures

Jin Quanbin[1] Liu Zhibin[1] Lu Liangliang[1] Zhang Yun[2] Luo Tingyi[2] Tang Yasen[2]

([1]Jiangsu Key Laboratory of Low Carbon and Sustainable Geotechnical Engineering, Southeast University, Nanjing 211189, China)

([2]Guangxi Beitou Construction and Investment Group Co., Ltd., Nanning 530028, China)

Abstract: Considering that copper mine tailings (CMTs) are commonly mixed with ordinary Portland cement, fly ash (FA), and kaolin to produce geopolymers, to make full use of CMTs, the properties of geopolymers manufactured under different material mass ratios and curing methods (standard curing, water bath curing, and 60 ℃ curing) are evaluated with significantly increased dosage of CMTs. Porosity and unconfined compressive strength tests, X-ray diffraction, field emission scanning electron microscopy, and energy dispersive spectroscopy are used to determine the physical and mechanical properties, microstructure, and mineral composition of geopolymers. Finally, costs and CO_2 emissions of specimens with different material mass ratios during the preparation processes are compared. The results show that during the geopolymerization of low-calcium materials, various geopolymer gels, including calcium silicate, calcium silicoaluminate, and mainly sodium silicoaluminate gels, coexist. The solid waste, cost, and carbon dioxide emission reductions can reach 100%, 166.3 yuan/t, and 73.3 kg/t, respectively. Under a curing condition of 60 ℃, the sample with a CMTs mass fraction of 70% and an FA mass fraction of 30% meets the requirements of porosity, compressive strength. The resource utilization of CMT and FA is realized in a more economical way.

Key words: copper mine tailings; geopolymer; solid wastes; characterization techniques; curing methods; carbon dioxide emission

DOI: 10.3969/j.issn.1003 - 7985.2024.03.009

According to the National Bureau of Statistics, refined copper production in 2023 was approximately 1.299×10^7 t. For every ton of refined copper produced, 2-3 t of copper slag and 196.5 t of tailings are discharged into the environment, mainly stored in tailings dams or underground[1]. Therefore, in 2023 alone, the discharge of copper mine tailings was approximately 2.55×10^9 t. This large amount of tailings generated by mining needs large disposal land and advanced sealing technology; therefore, the comprehensive utilization of tailings is currently one of the most concerning and challenging topics[2]. The amount of copper mine tailings (CMTs) has increased substantially during the last century because of the increased demand for copper and the improvements in processing/extraction techniques[3]. CMTs were classified as nonhazardous materials by the US Environmental Protection Agency in 1991 and the Basel Convention in 1996. As long as they meet regulatory requirements, CMTs can be freely used in various applications internationally, particularly in the construction industry, as alternative natural resources[4]. However, because of the lack of efficient, economical, and reasonable utilization methods, CMTs are predominantly deposited near mines and factories, occupying valuable land resources. Therefore, comprehensive research on the rapid reduction of CMTs in China is of utmost importance for environmental protection and economic benefits.

The studies on comprehensive utilization schemes mainly focus on cementing components, aggregates, and bricks[5-6]. The main alkali activators used are sodium hydroxide (SH), sodium silicate (SS), potassium hydroxide, and calcium oxide[7-8]. The addition of materials such as high-content ordinary Portland cement (OPC), natural sand, and silica fume improves the performance of concrete with slag[9]. Kundu et al.[6] suggest that the optimal replacement proportions of CMTs for OPC in cement concrete are 15% and 10%, respectively. The difference in the optimal replacement rate may be attributed to variations in how other materials are mixed and cured, but it does not substantially reduce OPC use. Either solid waste consumption is unsubstantial, or the environmental and economic benefits are insufficient. Reducing energy consumption and CO_2 emissions is particularly crucial because of the requirements for limiting carbon emissions. Moreover, the issue of natural sand as a nonrenewable resource must be addressed.

This study investigates the feasibility of producing

Received 2023-11-15, **Revised** 2024-03-19.

Biographies: Jin Quanbin (1993—), male, Ph. D. candidate; Liu Zhibin (corresponding author), male, doctor, professor, seulzb@seu.edu.cn.

Foundation items: The National Natural Science Foundation of China (No. 41877240), Scientific Research Foundation of Graduate School of Southeast University (No. YBPY1930).

Citation: Jin Quanbin, Liu Zhibin, Lu Liangliang, et al. Experimental study on the properties of CMTs-incorporated geopolymers prepared at low temperatures[J]. Journal of Southeast University (English Edition), 2024, 40(3): 295 - 303. DOI: 10.3969/j.issn.1003 - 7985.2024.03.009.

geopolymer bricks, which considerably enhance CMTs usage near ambient temperature. The study explores a simple combination of CMTs with other materials such as fly ash (FA), kaolin (KL), and OPC to completely replace natural aggregates and clay while substantially reducing the cement content. The selection of the optimal sample is based on factors such as unconfined compressive strength (UCS), porosity, economic viability, and CO_2 emissions. To evaluate the mechanical properties and microstructure of the specimens under different curing conditions (standard curing, water bath curing, and 60 ℃ curing), various tests were conducted, including UCS testing, water absorption analysis, porosity assessment, X-ray diffraction (XRD), field emission scanning electron microscopy (FESEM), and energy dispersive spectroscopy (EDS).

1 Experimental Program

1.1 Materials

The CMTs used in this study were obtained from Tongling, Anhui Province. Table 1 provides the main chemical composition of CMTs, OPC, FA, and KL (by weight percentage). The total sum of chemical compositions (SiO_2, Al_2O_3, and Fe_2O_3) in FA exceeds the minimum requirement of 70% for cementitious or pozzolanic action of class F FA. The CaO content of OPC is considerably higher than that of CMTs, FA and KL, while the Al_2O_3 composition is lower. Additionally, 98% pure commercial-grade SH flakes are used as the alkali activator.

Table 1 Main chemical composition of CMTs, OPC, FA, and KL %

Material	w(CaO)	w(SiO_2)	w(Al_2O_3)	w(MgO)	w(Na_2O)	w(SO_3)	w(K_2O)	w(S_2O_3)	w(Fe_2O_3)	w(P_2O_5)	w(TiO_2)	w(MnO)	w(CuO)
CMTs	5.57	53.21	13.32	1.21	0.17	3.84	3.59		8.98	0.32	0.41	0.34	0.18
OPC	63.40	19.40	4.80	1.50		1.70	1.20		4.30				
FA	5.60	45.10	24.20					2.10	0.85				
KL	0.50	55.00	45.00	0.30					0.01				

1.2 Mix design and procedure

The adopted mixture proportions are presented in Table 2, including the material mixing ratios and curing methods. The aim is to utilize CMTs mass fraction of more than 50% and OPC mass fraction of less than 10% to enhance CMTs usage and reduce the cement quantity. Moreover, previous tests indicated that specimens with CMTs mass fraction of more than 80% were challenging to achieve strength through self-compaction during curing. The water-to-materials ratio was 0.18, and the concentration of SH was 10 mol/L. These mixtures were used to prepare alkali-activated cylindrical CMTs geopolymers with a 50 mm diameter and 100 mm height.

Table 2 Mixture proportion %

Materials	S1	S2	S3	S4
CMTs	70	70	60	50
OPC	10			
FA	20	30	40	33
KL				17

CMTs, OPC, FA, and KL were mixed in a laboratory concrete mixer for 5 min at a speed of 22-24 r/min. The room-temperature SH solution was then added to the mixer and rotated for 3 min to obtain a homogeneous mixture[10]. The mixed slurry was poured into the mold, homogenized using a vibration table, and covered with a polyethylene sheet to prevent water loss[11]. Subsequently, all the specimens with molds were placed in a standard curing room for 24 h. Finally, the specimens were demolded and tested under different curing methods at various ages. Fig. 1 illustrates the mortar of S4 specimens cured at 60 ℃ after demolding. Standard curing refers to an environment with a temperature of (22 ± 2) ℃ and a relative humidity (RH) of (95 ± 5)%. Water bath curing involves immersing the specimen in water at (22 ± 2) ℃ under (95 ± 5)% RH air conditions. Similarly, 60 ℃ curing involves placing the specimen in an oven at 60 ℃.

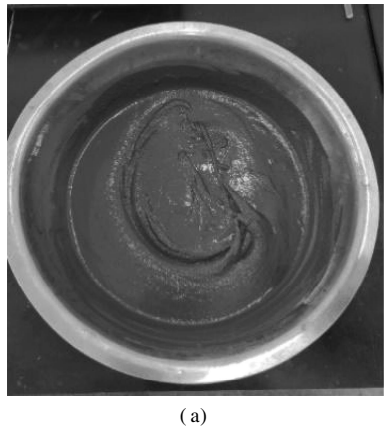

(a)

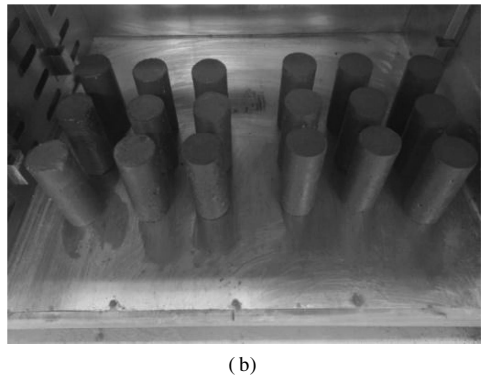

(b)

Fig. 1 S4 sample. (a) Mortar; (b) Samples cured at 60 ℃

1.3 Test methods

At different curing ages, the mechanical performance of the specimens was tested using the UCS test, the physical properties were tested using the water absorption and porosity test, and the mineralogical characterization and micromorphology were tested using XRD, FESEM, and EDS.

Water absorption and porosity tests were performed according to ASTM C642-21[12].

The UCS test was conducted at 7, 14, and 28 d to measure the strength variations of specimens with different material ratios under various curing conditions. Specimens retrieved from the curing room were covered with towels and tested promptly to prevent water exchange with the environment. Each specimen was subjected to the UCS test at a constant strain rate of 3 mm/min until the load values decreased with increasing strain or until a 15% strain was reached. The peak value of the UCS was recorded for each specimen[13].

XRD studies were applied to specimens under different curing conditions using Rigku-XRD (SmartLab) under the following conditions: Cu K_α is 0.154 178 nm; scanning speed is 5°/min; and scanning range 2θ is 10°-60°. The specimens were crushed into powder in an agate mortar and sieved with a 0.08 mm square-mesh sieve[14]. Then, specimens were heated for approximately 2 h at 80 ℃ to reduce the amount of adsorbed water[11]. Immediately after being removed from the oven, the specimens were tiled on the specimen stage and introduced into the vacuum system to test the chemical composition.

The micromorphology analysis of specimens was conducted using FESEM and EDS. Before FESEM and EDS analyses, the moisture-removed specimens were cut into slices 1-2 mm thick and coated with gold. The images were taken at approximately 2 000 × magnifications. FESEM and EDS analyses of specimens were conducted after 28 d of curing.

2 Results and Discussions

2.1 UCS analysis

Fig. 2 shows the UCS of four specimens (S1, S2, S3, and S4) at 7, 14, and 28 d of standard curing, water bath curing, and 60 ℃ curing. Overall, regardless of the curing condition, the specimen with OPC mass fraction of 10% exhibits the highest UCS. Under the 60 ℃ curing condition, this specimen surpasses the minimum compressive strength requirements for non-fired rubbish gangue brick specified in the Chinese standard JC/T 422—2007[15], reaching over 12 MPa. Conversely, the specimens without OPC display considerably lower UCS values. Among them, the specimen with KL (S4), which replaces a portion of FA, exhibits the lowest UCS. The addition of OPC greatly enhances the UCS of the specimen. This outcome is attributed to the increased concentration of calcium ions resulting from the OPC content, which facilitates alkali activator reactions with silicate ions, leading to more calcium silicate hydrate (C-S-H) formation. The EDS analysis in the following section further supports this explanation. Consequently, some researchers have sought to increase specimen strength by increasing the calcium ion concentration or curing temperature[9, 16].

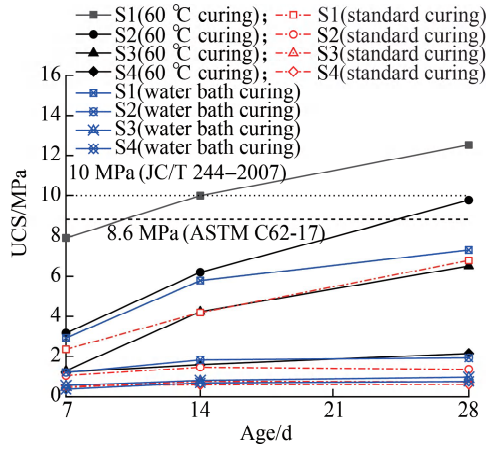

Fig. 2 UCS of samples at different curing ages under various curing conditions

Regarding the curing conditions, there is no significant difference in UCS between standard curing and water bath curing for all specimens. However, under the 60 ℃ curing condition, the UCS of all specimens shows considerable improvement. Geopolymerization involves dissolution and polycondensation as the main steps. Increasing the curing temperature accelerates the dissolution of silica and alumina species, promoting polycondensation[8]. When the FA proportion is increased from 30% to 40%, the Al ion content in the specimen also increases. Under 60 ℃ curing, despite a relatively small 10% reduction in CMTs (calcined marlstone) content, the UCS of the S2 specimen remains higher than that of the S3 specimen. Although KL contains higher Al ions, it has not been calcined at high temperatures (60 ℃) to achieve better pozzolanic activity. Test results demonstrate that even under an alkali activator and 60 ℃ curing conditions, KL struggles to exhibit sufficient cementitious properties, resulting in the lowest UCS among the specimens. Additionally, under the 60 ℃ curing condition for 28 d, the UCS of S1 and S2 meets the minimum individual compressive strength requirement for Grade negligible weathering building brick according to ASTM C62-17[17]. Although the UCS of the specimens mixed with FA (S2 and S3) is lower, it is considerably higher than that of the same specimens under other curing conditions. Analyzing the UCS growth rate of specimens under 60 ℃ curing (see Fig. 3), S1 exhibits rapid early strength growth (0-7 d), while S2 and S3 exhibit a higher growth rate during the

later curing stage (7-28 d). Notably, the UCS growth rate of S2 remains consistent during the 0-14 d and 14-28 d curing periods, indicating the potential for continued UCS growth beyond 28 d of curing. This result suggests that S2 and S3 require a longer curing period than S1 to achieve stable compressive strength. Because of the high pozzolanic reactivity of OPC, S1 demonstrates a relatively noticeable UCS growth rate even under standard curing and water bath curing. By extending the curing age (60 ℃), the minimum compressive strength requirements specified in the Chinese standard JC/T 422—2007[15] can be met for non-fired rubbish gangue brick.

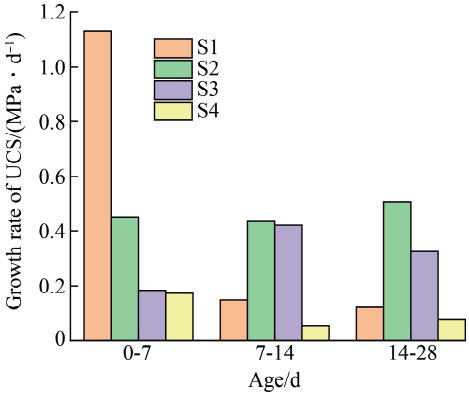

Fig. 3 Growth rates of UCS by samples under 60 ℃ curing

2.2 Analysis of water absorption and porosity

Fig. 4 illustrates the water absorption and porosity of each specimen under different curing conditions for 28 d. At a curing temperature of 60 ℃, all specimens meet the water absorption requirement of ASTM C62-17[17] for Grade SW (18%) after 5 h of boiling, which is identical to the maximum water absorption requirement for non-fired rubbish gangue brick (18%[15]). Only specimens S1 and S2 meet this requirement under other curing conditions. Additionally, the maximum water absorption of S1, S2, and S3 after 5 h of boiling under all three curing conditions meets the requirements of Grade MW (22%), except for S4 under standard and water bath curing. Moreover, under the curing condition of 60 ℃, the maximum 24-h cold water absorption of all specimens meets the minimum requirement of ASTM C902-22[18] for Class MX (14%), with S1 even meeting the minimum requirements of Class SX (8%). Based on the water absorption requirement of ASTM C902-22[18], the priority order of the specimens is S1, S2, S3, S4. The materials cured at 60 ℃ exhibit higher reactivity and more geopolymerization products, resulting in more compact specimens and lower porosity.

2.3 XRD analysis

Fig. 5 presents the XRD test results of each specimen under different curing conditions for 28 d. Under all curing

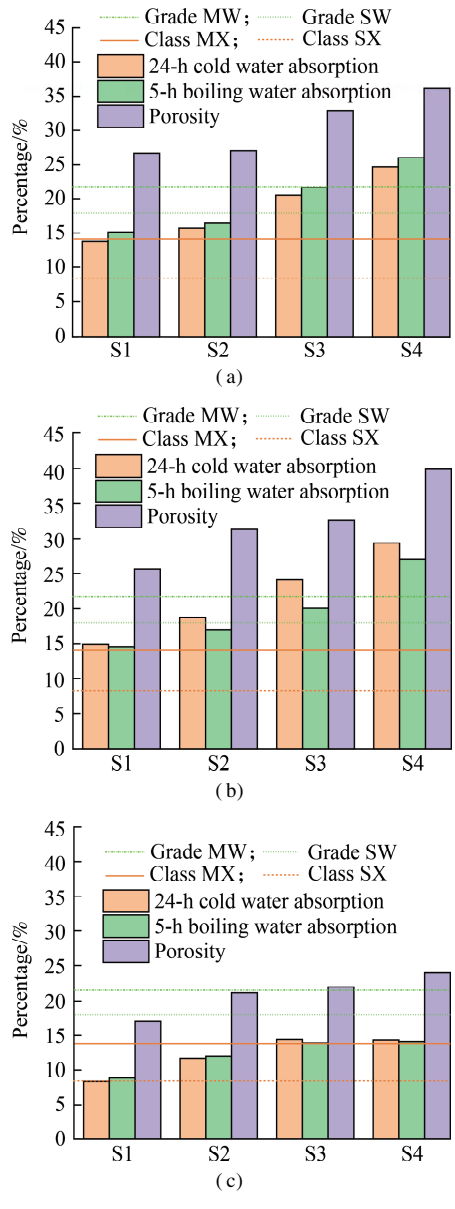

Fig. 4 Water absorption and porosity of the samples under different curing conditions for 28 d. (a) Standard curing; (b) Water bath curing; (c) 60 ℃ curing

conditions, CMTs primarily comprise crystalline materials with a substantial amount of silica, which aligns with the compositions shown in Table 2. The XRD analysis also reveals the presence of geopolymer gels (C-S-H, C-A-S-H, and N-A-S-H), quartz (SiO_2), and albite ($NaAlSi_3O_8$) minerals. This finding indicates the formation of C-S-H gel, contributing to the development of strength[19]. Furthermore, multiple geopolymer gels (C-S-H, C-A-S-H, and N-A-S-H) are observed, suggesting that during the hydration reaction, not all metal cations (Na^+) used to balance the electrical charge are completely replaced by Ca^{2+}, and some Si is replaced by Al. Notably, the XRD pattern of S4 exhibits a prominent peak of dolomite ($CaMg(CO_3)_2$) compared to other specimens because of the higher magnesium content in the KL. Notably, the geopolymerization process is accelerated under

the 60 ℃ curing condition for 28 d. In addition to geopolymer gel formation, the silica wave peak of S1 is lower than that of the other specimens, particularly at the peaks near 20°-30° and 50°. Despite the decrease in crystalline peak intensity, the patterns remain crystalline because of the partial dissolution of the mine tailings particles[8]. Additionally, the FESEM micrographs show that most particles only react on their surface and partially dissolve in the alkaline solution. However, under the three curing conditions, the corresponding peaks of S3 are slightly lower than those of S2, which can be attributed to the reduction in CMTs content leading to a decrease in Si content in S3.

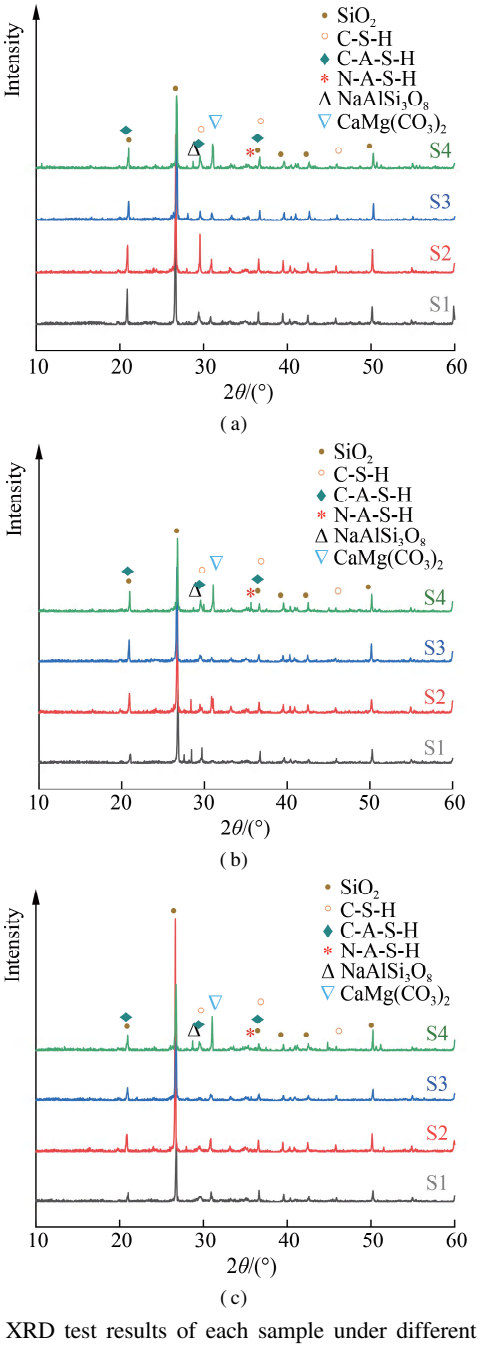

Fig. 5 XRD test results of each sample under different curing conditions for 28 d. (a) Standard curing; (b) Water bath curing; (c) 60 ℃ curing

2.4 FESEM and EDS analyses

Fig. 6 presents the morphological and microstructural features observed through FESEM of four specimens cured at 60 ℃ for 28 d. In Fig. 6(a), the geopolymeric gel is continuous and acts as a binder for the matrix. Needle-like products are seen within the holes, crossing each

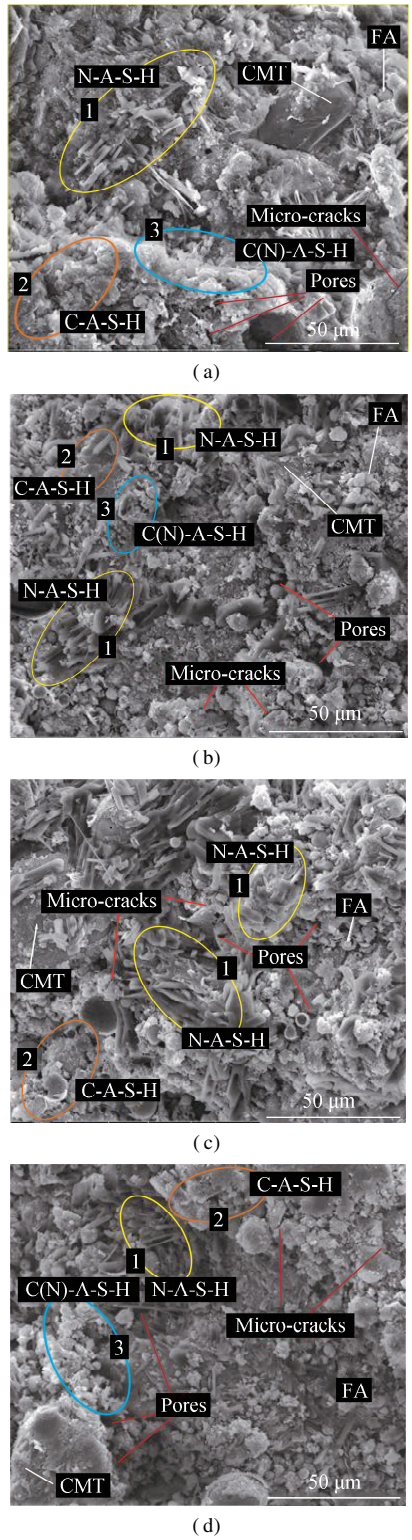

Fig. 6 FESEM micrographs of the chemical reaction products in different mortars. (a) S1; (b) S2; (c) S3; (d) S4

other and randomly arranged around cluster-like products. This observation aligns with the findings of Yan et al[14]. Some geopolymeric gels appear as independent particles, not tightly bonded with others (see Figs. 6(b)-(d)). During the microstructural examination, unreacted particles embedded within the matrix were observed, indicating incomplete dissolution of Al and Si. Additionally, cracks and holes resulting from the falling of FA particles were observed, possibly due to mechanical damage during specimen preparation for SEM observation or the curing conditions during the reaction process[14]. This observation indirectly suggests that when excessive FA is incorporated, some particles may not participate in geopolymerization and instead become attached to the geopolymer gels or detach. In comparison to Fig. 6(b), Fig. 6(c) shows that considerably more micro-cracks are found around unreacted FA particles as the FA content increases. Although the specimen in Fig. 6(d) has the same CMTs/FA mass ratio as that of Fig. 6(c), it contains a smaller total amount of FA. The morphology of FA exhibits a smooth texture with some micro-cracks, which can affect the strength of the geopolymer[20]. Thus, the morphology shows that S1 has better strength than the other specimens.

EDS testing was performed at the same position as that of Fig. 6 to analyze the main chemical reaction products. For simplicity, only the EDS test results of specimen S1 cured at 60 ℃ for 28 d are shown. Geopolymerization products are identifiable in different parts of Fig. 7(a). Analysis of Figs. 7(c)-(e) reveals that the main chemical reaction products detected in regions 1 and 2 have different sources. Geopolymerization products detected in region 2 are likely due to cement hydration, while those recognized in region 1 might result from pozzolanic reactions between copper slag and SH[21]. The EDS data plots (see Figs. 6(b)-(d)) clearly show that the geopolymerization products in region 1 have less calcium distribution compared to aluminum, sodium, and silicon, whereas region 2 has less sodium distribution. The inference of the XRD test results (see Fig. 5) is that region 1 mainly contains N-A-S-H, while region 2 mainly comprises C-A-S-H. Additionally, in the microscopic image of S1 with OPC, the coexistence of C-A-S-H gel and N-A-S-H gel in region 3 can be more clearly observed. EDS tests were also conducted on other specimens under the same curing conditions, and the same type of marks apparent in Fig. 6(a) are labeled in Figs. 6(b)-(d). The calcium content in the experimentally prepared specimens is low. In the FESEM image, the geopolymeric gels contained more N-A-S-H gel, consistent with the research findings of You et al. [22]. In terms of microstructure, specimens with a higher proportion of N-A-S-H gel exhibited more particle shedding and pores, while the S1 specimen containing more C-A-S-H gel showed considerably higher UCS than the other specimens. According to the above analysis, C-A-S-H gel improves the bearing capacity of the specimen structure more effectively than N-A-S-H gel.

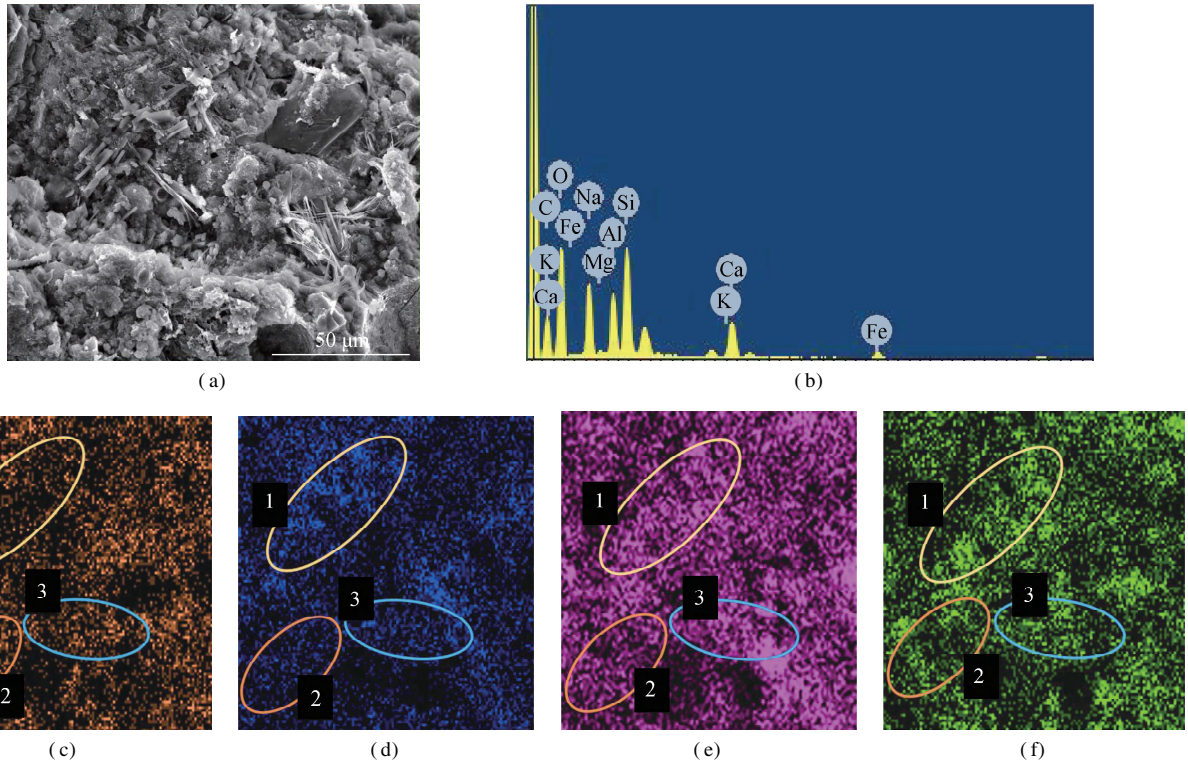

Fig. 7 SEM/EDS micrographs of S1 cured at 60 ℃ for 28 d. (a) SEM; (b) EDS; (c) EDS-Ca K; (d) EDS-Na K; (e) EDS-Al K; (f) EDS-Si K

2.5 Estimation of economics and CO_2 emission

Table 3 compares the costs and carbon dioxide emissions of the four specimens preparation processes. The well-performing specimens S1 and S2 were compared with brick specimens in Refs. [8, 23], denoted as B1 and B2. The estimated results are presented in Table 3. For specimens S1, S2, B1, and B2, 0.734 7, 0.816 3, 0.400 0, and 0.796 2 t of solid waste can be consumed per ton of specimen, respectively. The economic effects mainly depend on estimating the market price of CMTs/CS, OPC, SH, and nonrenewable materials and electricity costs during specimen curing. The costs of the four specimens are approximately 189.5, 166.3, 357.5, and 177.3 yuan/t. The total CO_2 emissions are calculated by summing the CO_2 emissions during the stages of OPC and SH production and specimen curing. The total CO_2 emissions of the four specimens are approximately 147.79, 73.3, 31.9, and 151.7 kg/t, respectively. B2 has relatively low CO_2 emission because the CO_2 emission during the exploitation of natural sand and clay is not estimated. Furthermore, according to Medina-Martos et al.[24], the main production method of commercial SH involves membrane cells, and the maximum CO_2-emission limit value per ton of SH is 1.958 t according to the regulations of the Standardization Administration of China. According to Amran et al.[25], the CO_2 emission from OPC production is 913 kg/t. Since specimens per ton are compared, the comparison of material freight and CO_2 emission during transportation is ignored. For the convenience of estimation, the form of power generation is assumed to be purely thermal, and the industrial power consumption is assumed to be 1 yuan/(kW·h).

The results show that S2 has the lowest cost. Compared with S1 and B2, S2 has a higher solid waste reduction, less SH usage, and the lowest CO_2 emission. Moreover, B1 consumes nonrenewable resources (natural sand and clay) and reduces solid waste by less than 1/2 compared to S2. Therefore, the S2 specimen has better cost performance. These estimation results indicate that the carbon footprint and life cycle assessment of the comprehensive application of different solid waste materials has considerable research importance.

Table 3 Summary of economic and CO_2 emission estimates

Sample label		S1	S2	B1[23]	B2[8]
Solid waste materials		70% CMTs, 20% FA	70% CMTs, 30% FA	40% CS	100% CMTs
OPC		10%	0	0	0
Nonrenewable material	Natural sand	0	0	21%	0
	Clay	0	0	39%	0
Alkali activator SH/t		0.036 7	0.036 7	0	0.076 4
Curing method		60 ℃, 28 d	60 ℃, 28 d	5 K/min, soaking at 1 025 ℃ for 1 h	90 ℃, 7 d
CO_2 emission/kg		147.79	73.3	31.9	151.7
Cost assessment/(yuan·t^{-1})		189.5	166.3	357.5	177.3

3 Conclusions

1) The specimen prepared with CMTs mass fraction of 70% and FA mass fraction of 30% (S2) under a curing temperature of 60 ℃ demonstrated several advantages, including 100% solid waste reduction, a cost of 166.3 yuan/t, and carbon dioxide emissions of 73.3 kg/t. Using CMTs in a more energy-efficient manner, it is feasible to produce environmentally friendly geopolymer bricks without using OPC, natural sand, or clay.

2) Compared to specimens containing 10% OPC, specimens without OPC required a longer curing age to reach the desired compressive strength. However, under a curing temperature of 60 ℃, the OPC-free specimens (S2 and S3) could meet the requirements for UCS and water absorption of bricks if given sufficient curing time. Among the three curing conditions (standard curing, water bath curing, and 60 ℃ curing), higher temperatures were found to promote geopolymerization of the specimens.

3) The decrease in the silica peak observed in the XRD results under similar silica contents indicates a greater involvement of silica in the geopolymerization process. During the geopolymerization of low-calcium materials, various geopolymer gels (C-S-H, C-A-S-H, and mainly N-A-S-H) were found to coexist. Additionally, the C-A-S-H gel had a greater influence on the growth of compressive strength.

4) As a building material, geopolymer tailings brick needs to meet the requirements of strength, porosity, and durability. The reactivity of tailings is very low, and when the strength is too low to meet the requirements, it can be increased by combining other methods, such as preloading. However, this tactic can greatly affect the porosity of the brick, making it difficult to meet the porosity requirements. Therefore, further study is warranted on the effect on the porosity, durability, and geopolymer reaction of geopolymer tailing brick that was further increased in strength by adopting various methods.

References

[1] Ince C, Derogar S, Gurkaya K, et al. Properties, durability and cost efficiency of cement and hydrated lime mortars reusing copper mine tailings of Lefke-Xeros in Cyprus[J]. *Construction and Building Materials*, 2021, **268**: 121070. DOI: 10.1016/j.conbuildmat.2020.121070.

[2] Behera S K, Mishra D P, Prashant S, et al. Utilization of mill tailings, fly ash and slag as mine paste backfill material: Review and future perspective[J]. *Construction and Building Materials*, 2021, **309**: 125120. DOI: 10.1016/j.conbuildmat.2021.125120.

[3] Nikvar-Hassani A, Vashaghian H, Hodges R, et al. Production of green bricks from low-reactive copper mine tailings: Chemical and mechanical aspects[J]. *Construction and Building Materials*, 2022, **324**: 126695. DOI: 10.1016/j.conbuildmat.2022.126695.

[4] Dhir R K, de Brito J, Mangabhai R, et al. *Sustainable construction materials*: *Copper slag*[M]. Cambridge, UK: Woodhead Publishing, 2016: 279－308.

[5] Liu B, Pan G H, Gao M, et al. Influence of grinding aid on the grinding effect of iron tailings and hydration properties of blended cement[J]. *Journal of Southeast University* (*Natural Science Edition*), 2022, **52**(5): 907－916. DOI: 10.3969/j.issn.1001-0505.2022.05.011. (in Chinese)

[6] Kundu S, Aggarwal A, Mazumdar S, et al. Stabilization characteristics of copper mine tailings through its utilization as a partial substitute for cement in concrete: Preliminary investigations[J]. *Environmental Earth Sciences*, 2016, **75**(3): 227. DOI: 10.1007/s12665-015-5089-9.

[7] Wang H R, Zhu Z D, Pu S Y, et al. Analysis on influencing factors of cadmium contaminated soil solidified by alkali-activated fly ash-slag[J]. *Journal of Southeast University* (*Natural Science Edition*), 2021, **51**(6): 1025－1032. DOI: 10.3969/j.issn.1001-0505.2021.06.015. (in Chinese)

[8] Ahmari S, Zhang L Y. Production of eco-friendly bricks from copper mine tailings through geopolymerization[J]. *Construction and Building Materials*, 2012, **29**: 323－331. DOI: 10.1016/j.conbuildmat.2011.10.048.

[9] Liu J Z, Sun W, Miao C W, et al. Effect of mineral admixtures on drying and autogenous shrinkage of concrete with low water-to-binder ratio[J]. *Journal of Southeast University* (*Natural Science Edition*), 2009, **39**(3): 580－585. DOI: 10.3969/j.issn.1001-0505.2009.03.030. (in Chinese)

[10] Sharma R, Khan R A. Sustainable use of copper slag in self compacting concrete containing supplementary cementitious materials[J]. *Journal of Cleaner Production*, 2017, **151**: 179－192. DOI: 10.1016/j.jclepro.2017.03.031.

[11] Sivasakthi M, Jeyalakshmi R, Rajamane N P. Fly ash geopolymer mortar: Impact of the substitution of river sand by copper slag as a fine aggregate on its thermal resistance properties[J]. *Journal of Cleaner Production*, 2021, **279**: 123766. DOI: 10.1016/j.jclepro.2020.123766.

[12] American Society for Testing and Materials. Standard test method for density, absorption, and voids in hardened concrete: ASTM C642-21[S]. West Conshohocken, PA, USA: American Society for Testing and Materials, 2021.

[13] American Society for Testing and Materials. Standard test method for unconfined compressive strength of cohesive soil: ASTM D2166/D2166M-16[S]. West Conshohocken, PA, USA: American Society for Testing and Materials, 2016.

[14] Yan Z H, Sun Z P, Yang J B, et al. Mechanical performance and reaction mechanism of copper slag activated with sodium silicate or sodium hydroxide[J]. *Construction and Building Materials*, 2021, **266**: 120900. DOI: 10.1016/j.conbuildmat.2020.120900.

[15] National Development and Reform Commission. Non-fired rubbish gangue brick: JC/T 422—2007[S]. Beijing, China: National Development and Reform Commission, 2008.

[16] Arıöz Ö, Kilinç K, Tuncan M, et al. Physical, mechanical and micro-structural properties of F type fly-ash based geopolymeric bricks produced by pressure forming process[J]. *Advances in Science and Technology*, 2010, **69**: 69－74. DOI: 10.4028/www.scientific.net/AST.69.69.

[17] American Society for Testing and Materials. Standard specification for building brick (solid masonry units made from clay or shale): ASTM C62-17[S]. West Conshohocken, PA, USA: American Society for Testing and Materials, 2017.

[18] American Society for Testing and Materials. Standard specification for pedestrian and light traffic paving brick: ASTM C902-22[S]. West Conshohocken, PA, USA: American Society for Testing and Materials, 2022.

[19] Usha, Nachiar S. Experimental study on the properties of concrete with replacement of cement by quarry sludge[J]. *International Journal of Engineering and Technical Research*, 2016, **5**(3): 813－817. DOI: 10.17577/ijertv5is031208.

[20] Khan K A, Raut A, Chandrudu C R, et al. Design and development of sustainable geopolymer using industrial copper byproduct[J]. *Journal of Cleaner Production*, 2021, **278**: 123565. DOI: 10.1016/j.jclepro.2020.123565.

[21] Najimi M, Sobhani J, Pourkhorshidi A R. Durability of copper slag contained concrete exposed to sulfate attack[J]. *Construction and Building Materials*, 2011, **25**(4): 1895－1905. DOI: 10.1016/j.conbuildmat.2010.11.067.

[22] You N Q, Liu Y C, Gu D W, et al. Rheology, shrinkage and pore structure of alkali-activated slag-fly ash mortar incorporating copper slag as fine aggregate[J]. *Construction and Building Materials*, 2020, **242**: 118029. DOI: 10.1016/j.conbuildmat.2020.118029.

[23] Marghussian V K, Maghsoodipoor A. Fabrication of unglazed floor tiles containing Iranian copper slags[J]. *Ceramics International*, 1999, **25**(7): 617－622. DOI: 10.1016/s0272-8842(98)00075-3.

[24] Medina-Martos E, Gálvez-Martos J L, Almarza J, et al. Environmental and economic performance of carbon capture with sodium hydroxide[J]. *Journal of CO_2 Utilization*, 2022, **60**: 101991. DOI: 10.1016/j.jcou.2022.101991.

[25] Amran M, Makul N, Fediuk R, et al. Global carbon recoverability experiences from the cement industry[J]. *Case Studies in Construction Materials*, 2022, **17**: e01439. DOI: 10.1016/j.cscm.2022.e01439.

低温制备含铜尾矿地聚合物性能试验研究

金权斌[1] 刘志彬[1] 鹿亮亮[1] 张 云[2] 罗婷倚[2] 唐亚森[2]

([1] 东南大学江苏省低碳与绿色岩土工程重点实验室, 南京 211189)

([2] 广西北投建设投资集团有限公司, 南宁 530028)

摘要:考虑到铜尾矿(CMTs)通常与普通硅酸盐水泥、粉煤灰(FA)和高岭土混合制成地聚合物,为了充分利用 CMTs,在显著增加 CMTs 用量的情况下,对不同材料质量配比和养护方式(标准养护、水浴养护和 60 ℃养护)下制备的地聚合物的性能进行了评价. 采用孔隙率和无侧限抗压强度测试、X 射线衍射、场发射扫描电镜和能量色散光谱来确定地聚合物的物理力学性能、微观结构和矿物成分. 此外,比较了不同材料质量配比的试样在制备过程中的成本和二氧化碳排放量. 结果表明,在低钙材料地聚合过程中,多种地聚合物凝胶共存,包括硅酸钙、硅铝酸钙,主要是硅铝酸钠凝胶. 固废消减、成本、二氧化碳排放量分别可达到 100%、166.3 元/t、73.3 kg/t. 在 60 ℃的养护条件下,含有质量分数 30% FA 和 70% CMTs 的试样可以满足砖孔隙率和抗压强度的要求,并且以更经济减碳的方式实现了铜尾矿和粉煤灰的资源化利用.

关键词:铜尾矿;地聚合物;固体废弃物;表征技术;养护方法;二氧化碳排放量

中图分类号:TU526